

# COMBUSTION OF NEAR STOICHIOMETRIC HYDROGEN-AIR MIXTURES STABILIZED NEAR TUBULAR POROUS BURNER

V. Bykov<sup>1\*</sup>, V. Gubernov<sup>2</sup>, U. Maas<sup>1</sup>

<sup>1</sup>Karlsruhe Institute of Technology (KIT), Institute of Technical Thermodynamics, Engelbert-Arnold-Strasse 4, Building 10.91 D-76131 Karlsruhe, Germany

<sup>2</sup>P.N. Lebedev Physical Institute of Russian Academy of Sciences, 53 Leninskiy ave, Moscow

## Abstract

In this paper, the effect of flame stabilization within tubular burners is investigated numerically. Two main regimes of combustion are observed - stabilized flames near the surface, called attached flame regime, and a detached flame. In the case of the attached flame regime the strain of the flow stabilizes the flame front, which exists in a very wide range of inflow rates. In the case of the detached flame regime joint effect of the strain, the curvature and diverging outflow influences the flame front. Three additional sub-regimes are reported in this case. Steady strain flames are found at relative low pressures and for lean mixtures. Then, with the increase of the inflow rate the steady flame front becomes unstable and flame oscillations emerge in a near stoichiometric mixture composition when the pressure is increased. This loss of stability is extremely sensitive to the ambient pressure, molecular diffusion and chemical kinetic. Further increase of the inflow rate stabilizes the flame again until another critical strain is attained and the flame quenches. The parametric range of these different regimes is outlined and critical inflow velocities are determined.

*Keywords:* premixed combustion, laminar strained flames, hydrogen combustion system, thermo-diffusive instability.

## 1. Introduction

Investigation of stretched and curved laminar flames in one of the central problems in both laminar and turbulent combustion [1, 2]. There is an enormous amount of literature devoted to experimental, analytical and numerical studies of the effect of stretch and curvature on the flame characteristics [3, 4]. The most attractive are those configurations which allow the one-dimensional formulation, like the counter flow planar and spherical/cylindrical flames. These configurations give an opportunity to single out the pure stretch and curvature phenomena, respectively.

A significant knowledge has been gained and accumulated for these systems, another system – tubular flames, which has been to large extent overlooked in the past and which allows to investigate the combined effect of stretch and curvature, becomes very interesting. As it is demonstrated in [1, 2], the tubular configuration can be formulated on a basis of a single spatial

dimension adopting a Lagrangian coordinate transformation. This drastically simplifies the numerical analysis of such systems. Experiments with tubular flames [5-7] demonstrated that stretch rates comparable to the flat counter-flow configuration can be attained for tubular flames. At the same time, the flame diameter at the extinction conditions can be of the order of millimeter, which is smaller than the length of recombination zone in hydrocarbon flames. Such a flame curvature can not be achieved in burner stabilized systems [8]. Thus the tubular flame configuration gives an opportunity to investigate the interplay of stretch and flame curvature in a geometrically simple and unique, in terms of parameter values, system.

Most of the papers devoted to tubular flames analyze the extinction characteristics of steady cylindrical reaction fronts [5-7, 9-12]. Hydrogen, methane and propane are considered as fuel. Air and mixtures of oxygen and nitrogen, argon, carbon dioxide – as an oxidizer. It is found that preferential diffusion plays a crucial role in the

\**Ответственный автор*  
E-mail: viatcheslav.bykov@kit.edu (V. Bykov)

near extinction behavior. In particular, flames with Lewis numbers smaller than one become stronger in response to flow induced contraction. The burned temperature exceeds the adiabatic temperature, while the diameter for extinction can be fairly small. The critical equivalence ratio for the extinction strain rate shifts to leaner compositions in comparison to the at counter-flow configuration [13]. In the case of the mixtures with Lewis number close or greater than one the reverse behavior takes place i.e. the burner temperature is comparable or smaller than the adiabatic one and the flammability limit extension is not observed.

It is known that the variation of the Lewis number may induce the onset of the thermo-diffusive instabilities. In the case of the freely propagating flame a linear stability analysis shows that planar flames can lose stability forming cellular (for Lewis number less than 1) and pulsating (for Lewis number greater than 1) instability [14]. The onset of cellular instabilities in tubular flames is investigated in [12] for the case of hydrogen and methane flames. It is shown that petal or corrugated flame structures can emerge as a result of the cellular thermo-diffusive instability. The onset of flame pulsations in tubular flame configuration has not been studied yet and this is the main goal of our current work. Flame pulsations are not only interesting nonlinear dynamical phenomena by themselves, they are also known to promote the onset of flame extinction [15, 16] and can be used in verification of the reaction mechanisms [17]. Thus the analysis of the conditions for emergence of flame oscillations and of their characteristics are of both applied and fundamental importance.

In the current paper, the effect of curvature on the emergence of pulsating diffusive-thermal instabilities and dynamics of flame oscillations similar to [18, 19] is in the focus of computational study. In order to undertake such analysis a tubular burner configuration is employed. The emergence of pulsating solutions near the stoichiometric

compositions of hydrogen-air systems is reported. A detailed study of the characteristics and critical parameters for the onset of flame oscillations for hydrogen-air flames is performed. First, the mathematical model is presented and discussed together with main physical assumptions made to treat the phenomenon in one spatial dimension. Then a numerical method and computational procedure to address the considered configuration is briefly outlined. In the results section four different regimes of the flames observed are described, characterized and the domain of their existence and emergence estimated. The reported regimes can be roughly subdivided into attached and detached flame front regimes. The latter can be further divided into steady, pulsating and strained near extinction limit flames. All these phenomena emerge in a very wide range of inflow rates. Thus bifurcation system parameters – critical values of the onset of different regimes represent a particular interest for further validation of physical sub-models used to describe combustion of hydrogen systems. The latter motivates the current study.

## 2. Mathematical model

The burner is considered to be infinite along the direction of symmetry ( $z$ -axis) in cylindrical coordinates (see Fig. 1). The mathematical model and numerical algorithm for solving the system of the governing equations employed in the current work are based on a formulation of the governing equation system for tubular flames [20] and reformulated using the derivation of a one-parameter-formulation for unsteady processes described in [21]. Starting with the governing equations for a two-dimensional axisymmetric configuration and using the assumptions (see e.g. [21] for more details)

- vanishing gradients of  $\mathcal{W}_i; T$  in  $z$ -direction
- $v_r$  is only a function of  $r$
- $v_x = zG(r)$
- $v_z = G(r)$

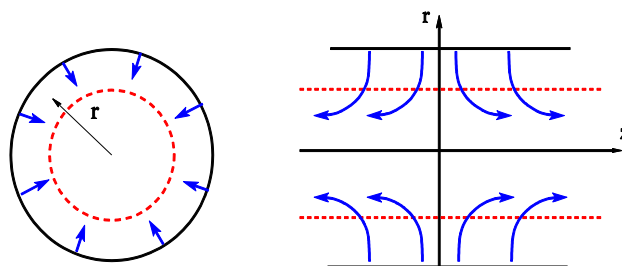


Fig. 1. Schematic illustration of the tubular flame configuration.

- neglecting dissipative terms in the energy equation
- assuming that pressure variations are negligible for the balance in the energy equation (quasi-uniform pressure assumption, low Mach number approximation)
- the axial pressure gradient is assumed to obey  $(1/z)\partial p = \partial z = J = const$ :
- the system behaves like an ideal gas law  $P = \rho RT = M$ , which is considered to be a good

approximations for the problems considered in this paper.

We end up with a system of equations consisting of the continuity equation, the equation for  $G = v_z = z$ , the species conservation equation and the energy equation. The system is closed by the ideal gas equation. Note that there is no need to solve for the radial velocity component, because J is related to G via the boundary condition.

$$J = -\rho_{r=R_0} \left( G_{r=R_0}^2 + \left( \frac{\partial G}{\partial t} \right)_{r=R_0} \right). \tag{1}$$

A system of conservation equations with detailed chemical reaction mechanisms and detailed transport models is considered. Then the system of governing equations can be written as

The detailed molecular transport is based on the Curtiss-Hirschfelder approximation [22, 23] including thermal diffusion (Soret effect) (see e.g. [24]) by

$$\frac{\partial p}{\partial t} + \frac{1}{r} \frac{\partial}{\partial r} (r \rho v_r) + \rho G(r) = 0$$

$$\frac{\partial G(r)}{\partial t} + \frac{1}{\rho z} \frac{\partial P}{\partial z} + v_r \frac{\partial G(r)}{\partial r} + G(r)^2 - \frac{1}{\rho} \left( \frac{1}{r} \frac{\partial}{\partial r} \left( r \mu \frac{\partial G(r)}{\partial r} \right) \right) = 0 \tag{2}$$

$$\frac{\partial w_i}{\partial t} = \frac{\dot{\omega}_i M_i}{\rho} - v_r \frac{\partial w_i}{\partial r} + \frac{1}{\rho r} \frac{\partial}{\partial r} r \left( \rho D_i^D \frac{w_i}{x_i} \frac{\partial x_i}{\partial r} + \frac{D_i^T}{T} \frac{\partial T}{\partial r} \right) \tag{3}$$

$$\frac{\partial T}{\partial t} = -\frac{1}{\rho C_p} \sum_{i=1}^{n_s} \dot{\omega}_i h_i M_i + \frac{1}{\rho C_p} \left( \frac{1}{r} \frac{\partial}{\partial r} \left( r \lambda \frac{\partial T}{\partial r} \right) \right) \tag{4}$$

$$- \frac{1}{\rho C_p} \sum_{i=1}^{n_s} c_{pi} \left( j_{i,r} \frac{\partial T}{\partial r} \right) - v_r \frac{\partial T}{\partial r}. \tag{5}$$

$$j_{i,r} = \rho D_i^D \frac{w_i}{x_i} \frac{\partial x_i}{\partial r} + \frac{D_i^T}{T} \frac{\partial T}{\partial r}. \tag{6}$$

In these equations  $t$  and  $r$  are the time and radius in cylindrical coordinates,  $T$  is the temperature,  $\omega_i$  is the mass fraction and  $x_i$  the mole fraction of species  $i$ ;  $\lambda$ ,  $c_p$ , and  $\lambda$  are the density, the constant pressure specific heat capacity, and the heat conductivity of the mixture, respectively;  $c_{pi}$ ,  $M_i$ ,  $\omega_i$ ,  $h_i$ , and  $j_i$  are the constant pressure specific heat capacity, the molar mass, the chemical rate of production, the specific enthalpy, and the diffusion

ux density of species  $i$ .  $M$  is the mean molar mass,  $D_i^D$  the diffusion coefficient for species  $i$ , and  $D^T$  is the thermal diffusion coefficient.

The burner has a large thermal inertia and thickness. Thus, it is assumed that the porous medium of the burner remains at constant temperature  $T_0$  i.e. the burner is thermally stabilized.

The boundary conditions are given as [25]

$$T = T_0, \quad \rho_0 v_0 (w_i - w_i^0) + j_i = \omega_i^s, \quad r = R_0$$

$$\frac{\partial T}{\partial r} = 0, \quad \frac{\partial Y_i}{\partial r} = 0, \quad r = 0. \tag{7}$$

where  $\omega_i^o$  denotes the mass fraction of species  $i$  in the fresh mixture, which is fed into the burner and  $\rho_0 v_0$  is the mass flux density of the fresh mixture.  $\omega_i^s$  is a surface reaction rate (accounting e.g. for the destruction of radicals at the burner surface), which is in this work assumed to be zero, because the pressure is relatively high, the surface of the burner is cold ( $T_0 = 298$  K) and flames considered are typically far away from the burner surface. These mixed boundary conditions account for the flux of the mass fraction of species at the burner entrance, diffusive flux and chemical reaction taking place at  $r = R_0$ . The temperature of the fresh mixture at  $R_0$  is assumed to be equal to the burner temperature  $T_0$ . The dominating mechanism of the heat loss from the reaction front is supposed to be due to the thermal interaction of the solid wall of the burner and the combustion front. The body forces are assumed to be negligible.

In this work we use the Warnatz mechanism [21, 24] which includes 38 elementary re-actions taking place between nine species ( $H_2$ , H,  $H_2O$ ,  $H_2O_2$ ,  $OH_2$ ,  $N_2$ , O,  $O_2$ , OH). This mechanism is considered as a representative example only. In the investigations made the outcome should not be qualitatively affected by the usage of a particular mechanism, however, as it is shown below the phenomenon is very sensitive to system parameters. The onset of pulsating regimes and their characteristics scatter the system states in the composition space which signifies dependence of the critical phenomena on the chemistry and diffusion properties of the mixture.

### 3. Numerical method

In order to simplify the numerical treatment the time derivative of  $\rho$  in the continuity equation Eq. (2) is replaced based on the ideal gas equation according to

$$\frac{\partial \rho}{\partial t} = -\frac{\rho}{T} \frac{\partial T}{\partial t} - \rho \bar{M} \sum_{i=1}^{n_s} \frac{1}{M_i} \frac{\partial w_i}{\partial t}, \quad (8)$$

where  $\bar{M}$  denotes the mean molar mass, and the right hand side of the equations are used. In this way the continuity equation no longer involves an explicit time derivative, and after spatial discretization Eq. (2) results in an algebraic equation.

A spatial discretization of the partial differential equation system on a non-equidistant grid using finite differences (central differences for the transport terms and upwind differences for the

convective terms) results in a large differential/algebraic equation system, which is solved by the linearly implicit extrapolation method LIMEX [26, 27] with error, order, and step size control. The spatial grid is statically adapted based on the magnitude of the local gradients and curvature of the dependent variables (see [24] for details). This altogether allows to integrate the system very accurately both in time and in space, which is very crucial for transient flame propagation regimes considered in the study.

In the numerical computations the temperature of the burner is in all cases -  $T_0 = 298$  K, while pressure -  $P$ , mass flux of the fresh mixture at the burner surface controlled by inflow velocity -  $v$ , and equivalence ratio -  $\phi$  are varied in the parametric study. The governing system of equations Eq. (2) is integrated numerically for the given parameters until the solution converges either to a steady combustion front, to an extinguished system or to a periodically pulsating solution. In the latter case, the time integration is stopped, once the periodic solution is found, i.e. when the amplitude of oscillations is not changing and e.g.  $x_i(x;t) = x_i(x;t + \tau)$  is satisfied, where  $\tau$  defines a period of flame oscillations and  $x_i$  is species mole fraction.

The initial solution profile is taken from the closest results obtained before in the parameter space - ( $P$ ,  $v$ ,  $\phi$ ). The loss of stability of the steady combustion fronts is analyzed numerically similar as described in [18, 19, 28].

Now, the main steps of the computational study are briefly outlined. All the control parameters ( $P$ ,  $v$ , and  $\phi$ ) are fixed except for one, namely,  $v$ . The solutions are integrated from the case of steady flame and  $v$  is gradually increased until flame pulsations occur. The amplitude of the oscillations is traced by choosing an observable variable (e.g.  $x_{OH}$ ) to monitor the time history and distinguish periodic behavior. The local maximum of  $x_{OH}$  distribution can be an example of such observable. The amplitude and frequencies of pulsations are analyzed as function of the bifurcation parameter -  $v$ . Note that the neutral stability boundary in the space of parameters can be found by repeating this procedure for different values of control parameters.

### 4. Results and discussion

The numerical analysis described above reveals that there are four regimes of combustion in the considered configuration of the cylindrical burner. For very small mass fluxes at the boundary the flame sheet is located very close to the surface of

the burner. We call this regime - burned stabilized or attached flame regime. The flame-wall thermal interaction (mainly heat loss) governs the behavior of combustion front in this case. For mass fluxes which are close to (or slightly exceeding) the mass flux of freely propagating flames the combustion front detaches from the burner surface and the radius of the location of the flame increases with  $v$ . The latter regime will be referred to as the detached flame.

#### 4.1. Attached flame regime

The attached flame behavior is illustrated in Fig. 2. The temperature, OH radical mole fraction and local gas flow velocity profiles are plotted for  $\phi = 1$ ,  $P = 4$  bar. This case is taken as a reference one throughout the exposition because it is representative to all parametric range investigated in this study. The main features of the regimes observed can be seen and outlined elaborately. For other set of parameters the observed regimes will only be shifted in the parameter space, but qualitatively will remain similar.

The radius of the burner is taken to  $R_0 = 5$  mm. The location of flame front is determined by the radius, at which the maximum mass fraction of OH radical is attained.

Figure 2 on the left shows temperature profiles of the steady flame fronts. A set of blue lines show the attached burner stabilized profiles with inflow velocities well below the laminar flame front such that heat losses to the walls influences dramatically the flame temperature. It drops almost by a factor

of two compared to the maximum value, but still reacting solutions are observed. One may conclude that even a small strain has stabilizing effect if compared to [28], where burner stabilized flame front on the external surface of cylindrical burner was investigated, presented and discussed. Next, the red profile represents a critical solution right before the flame detaches the surface. One can see a local maximum of temperature is attained near in this particular case. When the strain / inflow mass flux / inflow velocity is further increased the flame front detaches the surface (laminar velocity  $-v_l = 1.77$  (m/s) for this case), but remains steady with slight flame temperature decrease compare to the critical one shown by the red line.

Figure in the middle can be used to trace the position of the flame front and its structure for different inflow rates. One can see that by increasing the inflow rate the position of the maximum of OH (flame front position/distance) moves first towards the burner surface, it reaches a minimal value and then, similar as reported in e.g. [28], it increases until the flame detaches the burner surface. Note here a low maximum of OH mole fraction corresponds to low flame temperature regime having a lower inflow rate.

In the right sub-figure of Fig. 2 the gas local velocity profiles are shown such that the inflow rate corresponds to a boundary value. It shows additionally vast differences in the inflow rates between the attached, critical and detached regimes when they emerge. It can be seen that when the combustion front is attached to the surface of the burner the mass flow rate speeding

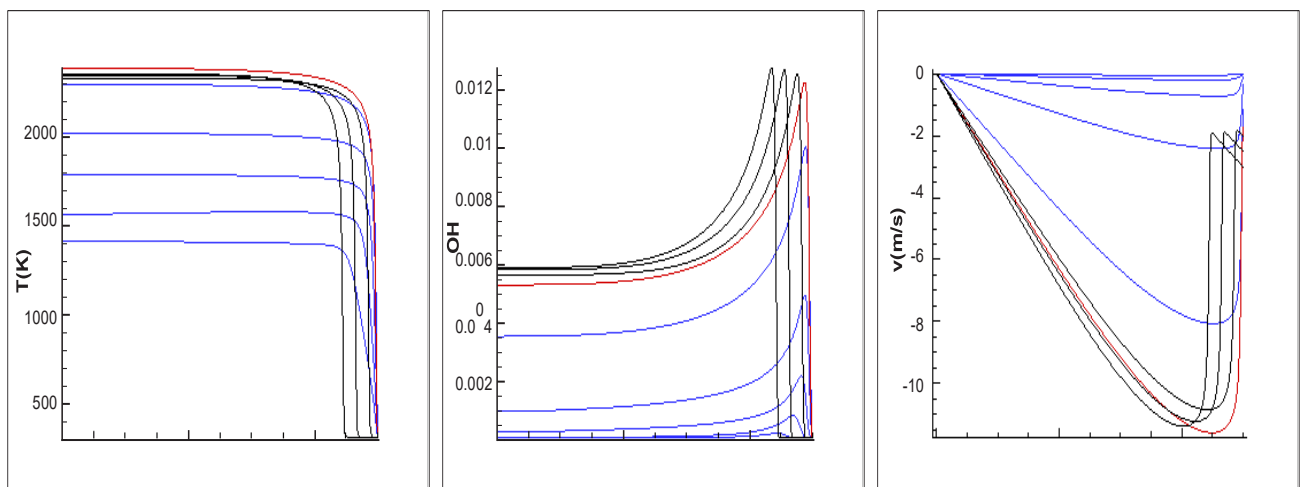


Fig. 2. The structure of the attached flame for  $\phi = 1$  and  $P = 4$  bar: (left) the flame temperature profiles; (middle) the OH mole fraction profiles; (right) the mass flux profiles; The solid red line shows the critical profile ( $v = -1.73$  (m/s)), while blue lines depict attached flame regime (with  $v = -1.55 \cdot 10^{-2}$ ;  $4.34 \cdot 10^{-2}$ ;  $1.27 \cdot 10^{-1}$ ;  $3.78 \cdot 10^{-1}$ ;  $1.17$  (m/s)) and black ones (for  $v = -2$ ;  $-2.5$ ;  $-2.75$  (m/s) respectively) illustrate the detached flame fronts profiles for moderate mass fluxes before the pulsating regime onsets.

up right at the surface (see blue and red curves), while the black lines show the detached regime and the gas flow first slows down before the flame front is reached. The local maximum corresponds approximately to the flame front velocity of the planar steady flames such that the balance establishes between both the mass flow rate coming from the surface and slowing down and the mass flux of products (in radial and in axial directions).

Note that for the attached regime (blue curves in all Figs. 2) higher the inflow rate leads to higher burned temperature and higher maximum of the OH mole fractions along the system solution profile. When the flame detaches the burner surface (red curve represent a critical moment) the situation changes the maximum of OH growth further while temperature drops down and the flame front position moves towards the symmetry line ( $r = 0$ ).

The stability of the steady attached flame is not in the focus of this study. It was investigated in detail in [28] and is not expected to be very different unless some very small radius of the tubular burner will be considered. This is because

of the burner radius is still large compared to the flame front width and the strain is very small for the attached regimes. Thus no large differences are expected between these configurations in the attached regime. Moreover, cases with very small radius are difficult to realize in real experiments and hence these remain beyond the scope of current computational study. The dependence of the critical mass flux for the onset of oscillations in the detached regime is the main focus of this study and is outlined in the following.

#### 4.2. Detached flame regimes

The detached strained flame can be further subdivided into steady, pulsating/oscillating and strained - near extinction regimes. When the critical condition (e.g. with respect to pressure) is not attained the flame front remains steady. As far as a critical condition is met the flame becomes unstable and oscillates in a wide range of system parameters. However, when the inflow rate is further increased it stabilizes the flame again and the flame front becomes stable again until the critical strain is reached and the flame quenches.

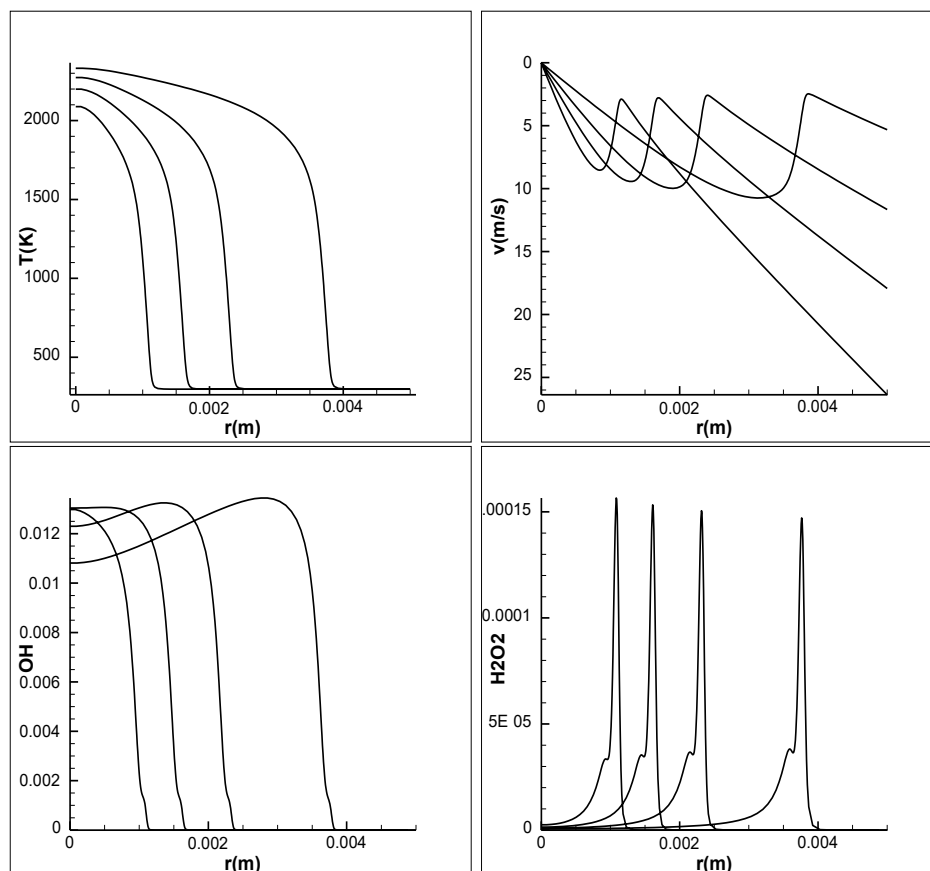


Fig. 3. The structure of the steady flame for  $\phi = 1$  and  $P = 1$  bar: the temperature, mass flow rate and OH with H<sub>2</sub>O<sub>2</sub> radicals are presented for  $v = -5.3, -11.6, -17.9, -26.3$  (m/s). Note here that the higher the inflow rate the closer the flame front (local maximum of the gas velocity profile) to the symmetry line.

#### 4.2.1. Strained steady flame regime

The steady flame front for all ranges of inflow rates is observed for the case e.g.  $\phi = 1$  for pressures below  $P \sim 3$  bar. Figures in fig. 3 show typical flame front structure and species profiles for steady flame for  $\phi = 1$  and  $P = 1$  in a wide range of inflow rates. Temperature profiles show how the flame temperature varies with the increase of the inflow rate. It drops down, while OH mole fraction grows and attains its maximum when the flame front comes closer to the symmetry line. One can see that in a wide range of inflow rates the flame structure remains qualitatively very similar (see e.g. the profile of the  $H_2O_2$  radical mole fraction) even the flame local mass flow rate at the flame front position does not change much. It signifies a balance between strain (in the diverging flow), curvature effects, chemical reaction and diffusion processes. Remark that all these effects coupled in a complicated manner can be studied in the transient combustion regime in detail by using the suggested configuration.

#### 4.2.2. Strained pulsating flame regime

With the increase of the pressure the flame front becomes thinner and instabilities emerge such that the flame starts periodically oscillating. Figures 4 show typical flame front structures for periodically oscillating regime. The onset of instabilities occurs near the position  $R = 4$  mm and persist for  $\phi = 1$  and  $P = 4$  in a wide range of mass flow rates and flame front positions / curvatures (see also Fig. 5). In percentage all system variables deviate in the similar range once a pulsating solution establishes (compare variations of all profiles presented in Figs. 4).

The periodic behavior is illustrated by representative state space variables – specie profiles, hydrodynamic properties are described by the gas flow velocity and the location of flame front can be traced by local maximum of the OH radical mole fraction.

Figures 5 show the range and character of the pulsating solutions in the whole range of system parameters of pulsating regimes. On the left figure

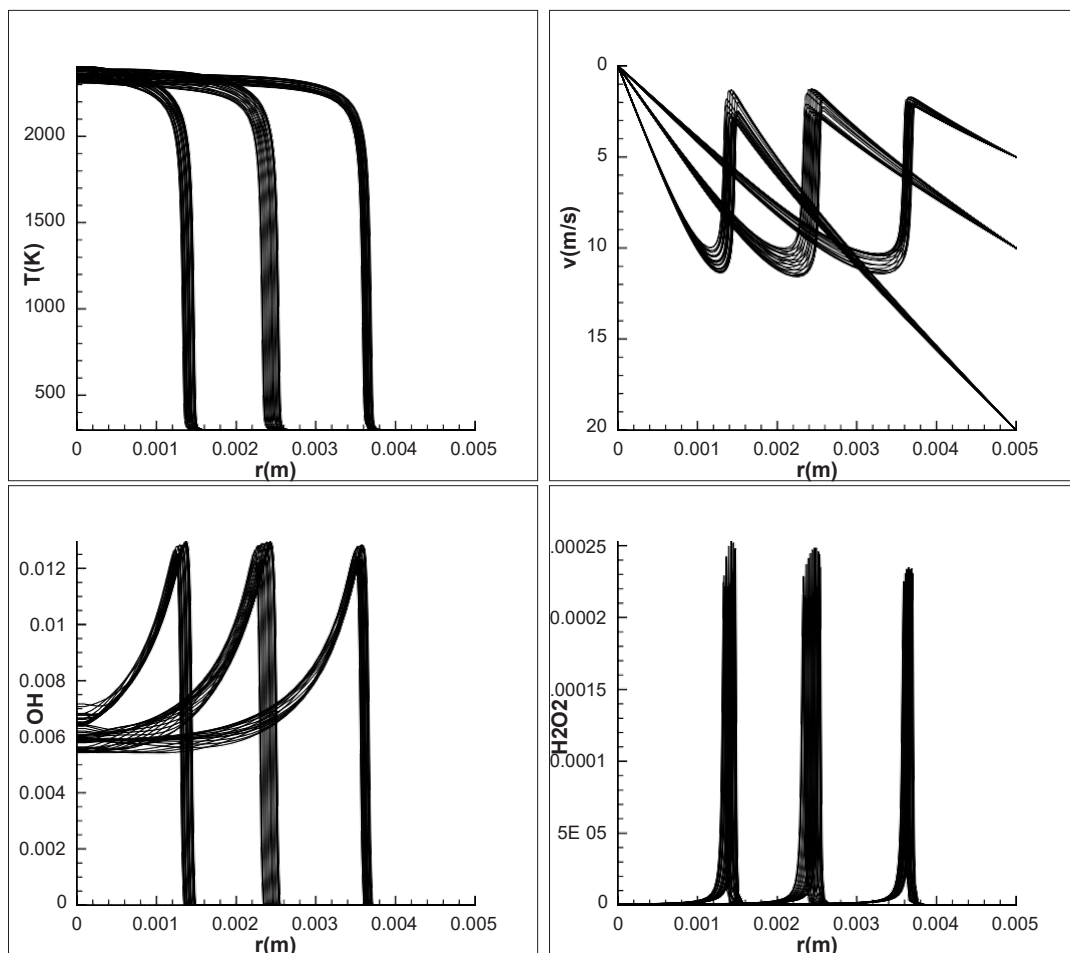


Fig. 4. The structure of the pulsating flame for  $\phi = 1$  and  $P = 4$  bar: the temperature, mass flow rate and OH with  $H_2O_2$  radicals are presented for the range of pulsating regimes -  $v = -5.0; 10.0; 20.0$  (m/s).

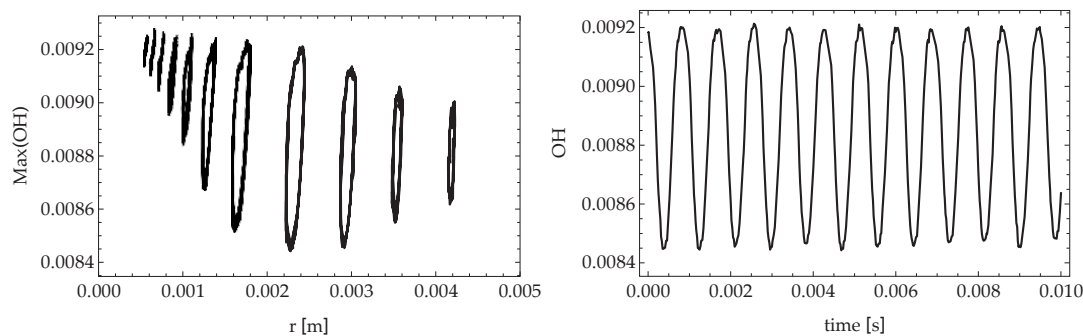


Fig. 5. The structure of the pulsating flame for  $\phi = 1$  and  $P = 4$  bar: (left) the maximum of the OH mole fraction along the system solution profile vs. radial coordinate for a range of  $v = -5.0, \dots, 60.0$  (m/s); (right) the maximum of the OH mole fraction along the time for pulsating solution with largest amplitude  $-v = -10.0$ .

one can see the maximum of OH along the solution profiles as function of special variable. The oscillations emerge at  $R \sim 4$  mm with already quite high amplitude (see the most right oscillating patterns of OH maximum), which increases and reaches its largest value around the middle of the radial distance (corresponding to  $v \sim 10$  (m/s)). The pulsations survive for very small radius of the flame front and very strong strain of the flow. Figure 5 on the right shows the time evolution of the OH maximum at this regime for several periods of oscillations. A very regular periodic oscillations are observed and reported.

Figures 6 present further the structure of pulsating flame in the state space of (H, OH) species mole fractions for their maximum values along the pulsating solutions. The figure on the left shows a typical pattern of an oscillating behavior illustrating the influence of pulsations on the thermo-chemical system state. The maximum of H mole fraction presented on the right figure illustrates additionally periodic character of the pulsating regime.

The results of the detailed computational analysis for the illustrative case of  $\phi = 1$  used to outline and describe the main observation

made are summarized in Figs. 7. Here on the left panel amplitudes of pulsations are shown for the pressures when the oscillation behavior emerges –  $P = 3; 4; 5$  bar. One can see the range is wide with the increase of the pressure as well as the amplitude steadily grows. For all range of pressures a maximum of the amplitudes is attained approximately at the same inflow rate. The figure on the right shows quite high values of frequency even at the point when the oscillations emerge. The frequency gradually increases with pressure though there is also a kind of saturation of the frequency with the pressure increase.

In Tab. 1 all obtained results of critical inflow rates for the onset of pulsations ( $v_1, v_2$ ) as well as for extinguishing strained flames ( $v_3$ ) are summarized. In the considered range of the equivalence ratio there is no pulsating regime for normal pressure is reported. With the pressure increase (near  $P = 2$ ) the flame front becomes unstable already for moderate values of the inflow rate. The interval of the pulsating solution grows with the pressure and reaches very high velocities of order of  $\sim 100$  (m/s).

The range of this interval reaches the maximum at the stoichiometric composition and narrows

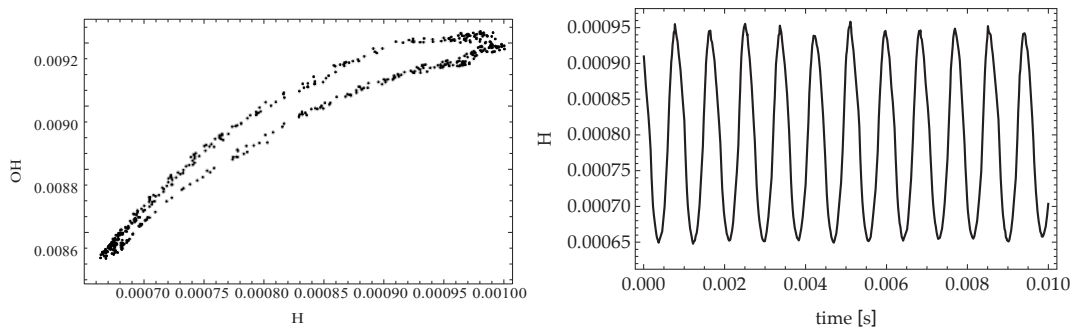


Fig. 6. The structure of the pulsating flame for  $\phi = 1$  and  $P = 4$  bar: (left) the maximum of the H mole fraction along the system solution profile; (right) the maximum of the H mole fraction along the time for pulsating solution with largest amplitude  $-v = -10.0$  (m/s).

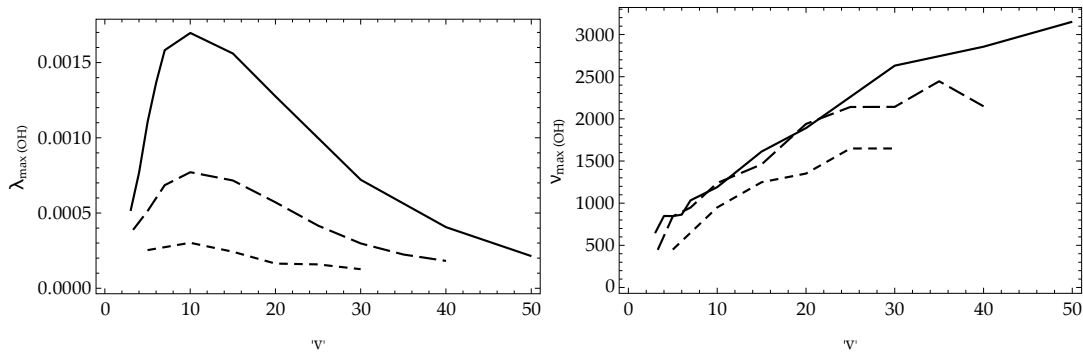


Fig. 7. The structure of the pulsating flame for  $\phi = 1$  and  $P = 3, 4, 5$  bar: (left) the amplitude of the maximum of the OH mole fraction in the range of pulsating solutions by  $v$  [m/s]; (right) the maximum of the OH mole fraction; Solid lines show  $P = 5$ , dashed lines represent results for  $P = 4$  and dotted lines show  $P = 3$  case.

towards leaner or richer mixtures. One can conclude the phenomena is very stable and can be easily observed and studied experimentally.

**4.2.3. Strained flames near extinction**

With further increase of the mass flow rate the flame stabilizes again until critical extinction limit is reached. At this critical values the strain rate is attained such that the residence time becomes

smaller than the characteristic time scale for chemical reaction to take place and the flame quenches.

Figures 8 summarize the typical stages near the extinction limit. Here we return to the case  $\phi = 1$  and  $P = 1$  bar simply because the flame front structure can be better seen for the case of lower pressure (the flame front is just wider). Similar as in figs. 3 the blue color shows steady profiles near the extinction limit, while the red one shows the

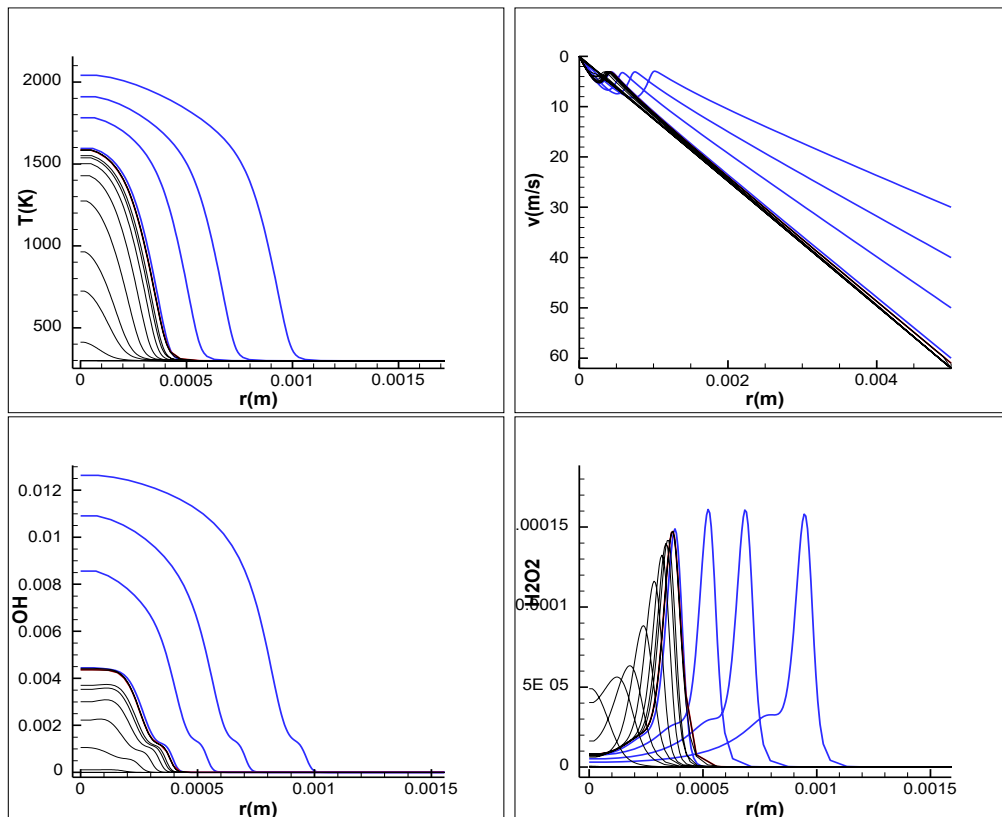


Fig. 8. The structure of the strained flame for  $\phi = 1$  and  $P = 1$  bar: the temperature, mass flow rate and OH with  $H_2O_2$  radicals are shown for the range of steady flame fronts with  $v = 30.0; 40.0; 50.0; 60.0$  shown by blue lines,  $v = 61.0$  - critical value shown by the red line while black solid lines represent transient extinguishing solution profiles for  $v = 62.0$ .

Table 1. Critical values of the absolute values of the inflow velocities; Cases -  $\phi = 1.25, 1, 0.75$

$\phi$	P	$V_1$	$V_2$	$V_3$
1.25	5	4.75	82.5	345
1.25	4	6.75	57.5	275
1.25	3	10.5	25	205
1.25	2	-	-	126
1.25	1	-	-	55
1.00	5	2.15	88	365
1.00	4	3.15	61.5	295
1.00	3	4.75	37.5	215
1.00	2	-	-	135
1.00	1	-	-	62
0.75	5	1.3	47.5	325
0.75	4	2.	37.5	255
0.75	3	3.75	22.5	195
0.75	2	6	8	120
0.75	1	-	-	55

profile for the critical inflow rate and the black thin lines illustrate how the extinction processes proceeds when the inflow rate slightly exceeds the limiting value. The inert solution emerges at the end. Remark that almost the same burning temperate is observed as in the case of the burner stabilized flame near very low inflow velocities.

Figure 9 finalizes the results and shows the fast range of critical inflow velocities of the strained extinction limits. It shows that the flame propagation phenomenon in near stoichiometric compositions represent a very stable combustion process.

Additionally, all different regimes reported cover several order of magnitude by the inflow rates (ranging from  $10^{-2}$  to  $10^2$  (m/s)), such that this geometry/configuration can be used as a substitute/generic configuration to study hydrogen combustion phenomena in all possible regimes, which can be observed in highly turbulent hydrogen flames, with all major effects of curvature, strain, heat losses taken into account. Moreover, these can be investigated «independently» and considered transiently when the system undergoes the transition between the meta-stable regimes of the flame propagation.

## 5. Conclusions

Two regimes of combustion front in a tubular burner configuration were reported: attached and detached flames. For relatively small mass

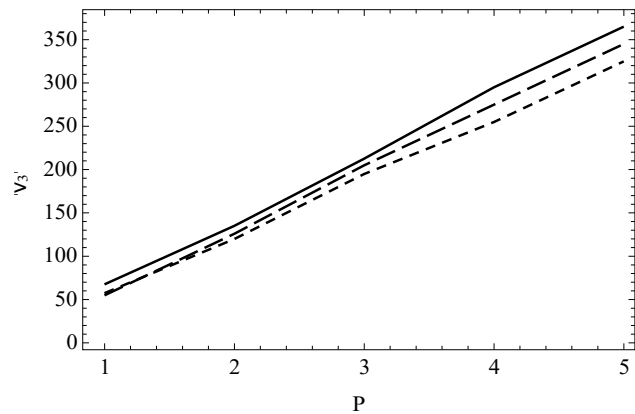


Fig. 9. Critical strain velocities for  $\phi = 0.75, 1.00, 1.25$  as function of pressure. Solid line for  $\phi = 1$ , dashed line represents results for  $\phi = 1.25$  and dotted lines show  $\phi = 0.75$  cases (see Tab. 1).

flow rates the flame front is located very close to the surface of the burner. The flame-wall thermal interaction (heat losses) governs the behavior of combustion front in this case. Because this regime is realized for very low velocities the attached flame regime is similar to the burner stabilized flames of the cylindrical burner studied before in [28]. In particular, similar behavior of the flame front is observed in this regime, namely, because the net heat flux from the combustion front to the surface burner increases the flame front further drifts away from the burner surface when the inflow rate decreases.

For inflow rates exceeding the mass flow rate of the freely propagating flame the combustion front detaches from the burner surface and flame radius reduces with the mass flux of the fresh mixture. In the case of moderate (but higher than a laminar flame) inflow rates and with increase of the pressure the critical velocities attained for the onset of instability and pulsating flames emerge. These were estimated and outlined for moderate pressures and near stoichiometric mixture compositions.

The change in the flame structure in the detached flame regime due to the curvature effect and strain significantly influence the flame stability characteristics. Even for critical pressures, further increase of inflow rates suppress the oscillations, amplitude decreases while the frequency of oscillations increase and flames are stabilized once again. The latter limit is also computed together with the critical velocities leading to strain rates at which the flame quenches.

The study has shown that the suggested configuration elaborates interplay between geometry/curvature, diffusion and chemistry.

This plays an important role in controlling the flame propagation and transition regimes. Thus it can be used as an additional generic set-up, which is very interesting and promising to further verify detailed chemical kinetics and diffusion models for hydrogen combustion processes in transient regimes.

### Acknowledgments

VB and UM authors acknowledge the support from DFG grant number BY 94/2-1 (DFG). VG acknowledges the support from Russian Science Foundation project No. 21-13-00434.

### References

- [1]. Dixon-Lewis G etc. (1991) Symposium (International) on Combustion 23:305-324. DOI: 10.1016/S0082-0784(06)80274-2
- [2]. Smooke M (1991) Dynamics of Deflagrations and Reactive Systems 131:125.
- [3]. Law CK (2010) Combustion physics, Cambridge university press, Cambridge, UK.
- [4]. Warnatz J, Maas U, Dibble RW, Warnatz J (2006) Combustion, Springer. ISBN-10 3-540-25992-9
- [5]. Ishizuka S (1989) An experimental study on extinction and stability of tubular flames, Comb. and Flame 75:367-379. DOI: 10.1016/0010-2180(89)90049-7
- [6]. Kobayashi H, Kitano M (1989) Combustion and Flame 76:285-295. DOI: 10.1016/0010-2180(89)90111-9
- [7]. Ogawa Y, Saito N, Liao C (1998) Burner diameter and flammability limit measured by tubular flame burner, in: Symposium (International) on Combustion, 27:3221-3227. DOI: 10.1016/S0082-0784(98)80186-0
- [8]. Kichatov B, Kolobov A, Gubernov V, Bykov V, Maas U (2020) Combustion Theory and Modelling 24:650-665. DOI: 10.1080/13647830.2020.1734238
- [9]. Mosbacher DM, Wehrmeyer JA, Pitz RW, Sung C-J, Byrd JL (2002) Proceedings of the Combustion Institute 29:1479-1486. DOI: 10.1016/S1540-7489(02)80181-X
- [10]. Hu S, Wang P, Pitz RW (2009) Proceedings of the Combustion Institute 32:1133-1140. DOI: 10.1016/j.proci.2008.06.183
- [11]. Hu S, Pitz RW, Wang P (2009) Combustion and Flame 156:90-98. DOI: 10.1016/j.combustflame.2008.09.004
- [12]. Wang P, Hu S, Pitz RW (2009) Proceedings of the Combustion Institute 32:1141-1147. DOI: 10.1016/j.proci.2008.07.012
- [13]. Fursenko R, Minaev S, Nakamura H, Tezuka T, Hasegawa S, Kobayashi T, Takase K, Katsuta M, Kikuchi M, Maruta K (2015) Combustion and flame 162:1712-1718. DOI: 10.1016/j.combustflame.2014.11.032
- [14]. Sivashinsky GI (1977) Combustion Science and Technology 15:137-145. DOI: 10.1080/00102207708946779
- [15]. Gubernov V, Kolobov A, Polezhaev A, Sidhu H, Mercer G (2010) Proc. Royal Society A: Mathematical, Physical and Engineering Sciences 466:2747-2769. DOI: 10.1098/rspa.2009.0668
- [16]. Kurdyumov VN, Gubernov VV (2020) Combustion and Flame 219 :349-358. DOI: 10.1016/j.combustflame.2020.06.014
- [17]. Nechipurenko S, Miroshnichenko T, Pestovskii N, Tskhai S, Kichatov B, Gubernov V, Bykov V, Maas U (2020) Combustion and Flame 213:202-210. DOI: 10.1016/j.combustflame.2019.12.016
- [18]. Gubernov VV, Bykov V, Maas U (2017) Combust. Flame 185:44-52. DOI: 10.1016/j.combustflame.2017.07.001
- [19]. Korsakova AI, Gubernov VV, Kolobov AV, Bykov V, Maas U (2016) Combust. Flame 163:478-486. DOI: 10.1016/j.combustflame.2015.10.024
- [20]. Dixon-Lewis G, Giovangigli V, Kee RJ, Miller JA, Rogg B, Smooke MD, Stahl G, Warnatz J (1991) Dynamics of Deagrations and Reactive Systems: Heterogeneous Combustion, Progress in Astronautics and Aeronautics (AIAA) Washington, DC 131:125-144. DOI: 10.2514/5.9781600866043.0125.0144
- [21]. Stahl G, Warnatz J (1991) Combust. Flame 85:285-299. DOI: 10.1016/0010-2180(91)90134-W
- [22]. Giovangigli V (1990) IM-PACT of Computing in Science and Engineering 2:73-97. DOI: 10.1016/0899-8248(90)90004-T
- [23]. Ern A, Giovangigli V (1994) Multicomponent transport algorithms, vol. 24, Springer, Berlin. DOI: 10.1007/978-3-540-48650-3

### Горение почти стехиометрических водородно-воздушных смесей, стабилизированных вблизи трубчатой пористой горелки

В. Быков<sup>1\*</sup>, В. Губернов<sup>2</sup>, У. Маас<sup>1</sup>

<sup>1</sup>Технологический институт Карлсруэ (ТИК), Институт технической термодинамики, Энгельберт-Арнольд-штрассе 4, корпус 10.91 D-76131 Карлсруэ, Германия

<sup>2</sup>Физический институт им. Б.Н. Лебедева Российской академии наук, Ленинский проспект, 53, Москва, Россия

## Аннотация

В данной работе эффект стабилизации пламени в трубчатых горелках исследуется численно. Наблюдаются два основных режима горения – стабилизированное пламя у поверхности, называемое режимом присоединенного пламени, и отошедшее пламя. В случае режима присоединенного пламени деформация потока стабилизирует фронт пламени, существующий в очень широком диапазоне скоростей притока. В случае отрывного режима пламени на фронт пламени влияет совместное влияние деформации, искривления и расходящегося потока. В этом случае сообщается о трех дополнительных подрежимах. Стационарное деформационное пламя наблюдается при относительно низких давлениях и для обедненных смесей. Затем с увеличением скорости натекания стационарный фронт пламени становится неустойчивым и возникают колебания пламени в составе смеси, близком к стехиометрическому, при повышении давления. Эта потеря стабильности чрезвычайно чувствительна к атмосферному давлению, молекулярной диффузии и химической кинетике. Дальнейшее увеличение скорости притока снова стабилизирует пламя до тех пор, пока не будет достигнуто новое критическое напряжение и пламя не погаснет. Очерчен параметрический диапазон этих различных режимов и определены критические скорости притока.

*Ключевые слова:* предварительно смешанное горение, ламинарное напряженное пламя, система горения водорода, термодиффузионная неустойчивость.

## Құбырлы кеуекті оттық жанында тұрақтандырылған дерлік стехиометриялық сутегі-ауа қоспаларының жануы

В. Быков<sup>1\*</sup>, В. Губернов<sup>2</sup>, У. Маас<sup>1</sup>

<sup>1</sup>Карлсруэ технологиялық институты (ТИК), Техникалық термодинамика институты, Энгельберт-Арнольд-страссе 4, корпус 10.91 D-76131 Карлсруэ, Германия

<sup>2</sup>Б.Н. Лебедев атындағы физикалық институт РФА, Ленин даңғылы, 53, Мәскеу, Ресей

## Аңдатпа

Бұл жұмыста құбырлы оттықтардағы жалынды тұрақтандырудың әсері сандық түрде

зерттеледі. Екі негізгі жану режимі байқалады – бекітілген жалын режимі деп аталатын бетке жақын тұрақтандырылған жалын және шегінетін жалын. Қосылған жалын режимі жағдайында ағынның деформациясы кіріс жылдамдығының өте кең диапазонында болатын жалын фронтын тұрақтандырады. Ажыратылған жалын режимі жағдайында жалын фронты деформацияның, қисықтықтың және дивергентті ағынның бірлескен әсерімен әсер етеді. Бұл жағдайда үш қосымша ішкі режим хабарланады. Тұрақты деформациялық жалын салыстырмалы түрде төмен қысымда және арық қоспалар үшін байқалады. Содан кейін ағып кету жылдамдығының жоғарылауымен стационарлық жалын фронты тұрақсыз болады және қысымның жоғарылауымен стехиометриялыққа жақын қоспаның құрамында жалынның тербелістері пайда болады. Бұл тұрақтылықтың жоғалуы атмосфералық қысымға, молекулалық диффузияға және химиялық кинетикаға өте сезімтал. Кіру жылдамдығының одан әрі жоғарылауы жаңа критикалық кернеуге жеткенше және жалын сөнгенше жалынды қайтадан тұрақтандырады. Осы әртүрлі режимдердің параметрлік диапазоны көрсетілген және ағынның критикалық жылдамдығы анықталады.

*Кілт сөздер:* алдын ала араластырылған жану, ламинарлы қарқынды жалын, сутегі жану жүйесі, термиялық диффузияның тұрақсыздығы.